

AMERICAN UNIVERSITY OF BEIRUT

ELECTROSPUN PVC/MOFS-AG NANOCOMPOSITES AS
EFFICIENT ANTIBACTERIAL MEMBRANES

by
MOHAMMAD AL-HADI HASHEM

A thesis
Submitted in partial fulfillment of the requirements
for the degree of Master of Science
to the Department of Mechanical Engineering
of the Maroun Semaan Faculty of Engineering and Architecture
at the American University of Beirut

Beirut, Lebanon
January 2023

AMERICAN UNIVERSITY OF BEIRUT

ELECTROSPUN PVC/MOFS-AG NANOCOMPOSITES AS
EFFICIENT ANTIBACTERIAL MEMBRANES

by
MOHAMMAD AL-HADI HASHEM

Approved by:



Dr. Mohammad Hmadeh, Associate Professor
Chemistry

Advisor



Dr. Kamel AbouGhali, Professor
Mechanical Engineering

Co-Advisor



Dr. Nessreen Ghaddar, Professor
Mechanical Engineering

Member of Committee



Dr. Mohammad Ahmad, Professor
Chemical Engineering

Member of Committee

Date of thesis defense: January 11th, 2023

AMERICAN UNIVERSITY OF BEIRUT

THESIS RELEASE FORM

Student Name: Hashem Mohammad Al-Hadi

Last First Middle

I authorize the American University of Beirut, to: (a) reproduce hard or electronic copies of my thesis; (b) include such copies in the archives and digital repositories of the University; and (c) make freely available such copies to third parties for research or educational purposes:

- As of the date of submission
- One year from the date of submission of my thesis.
- Two years from the date of submission of my thesis.
- Three years from the date of submission of my thesis.

Mohammad Al-Hadi
Hashem _____

17/1/2023 _____

Signature

Date

ACKNOWLEDGEMENTS

I would like to express my deepest appreciation to my committee advisors: Dr. Mohammad Hmadeh, Dr. Kamel AbouGhali, and Dr. Nessreen Ghaddar for their valuable support, encouragements, and patience throughout the research. It was a great privilege and honor to work under their supervision, and I am appreciative for what they offered me. I would like to also thank Dr. Mohammad N. Ahmad for his valuable commentaries as a member of the committee.

I would like to give a special thanks for my Family. I am forever grateful for such a caring, patient, and supportive family.

I would like also to acknowledge the financial support of the Masri Institute of Energy and Natural Resources and the University Research Board (URB) of the American University of Beirut. I am also thankful for the Kamal A. Shair Central Research Science Lab (KAS CRSL) of the Faculty of Arts and Sciences at AUB for providing access to their facilities.

ABSTRACT

Mohammad Al-Hadi Hashem

for

Master of Science

Major: Energy Studies

Title: Electrospun PVC/MOFS-AG Nanocomposites as Efficient Antibacterial Membranes

In this study, electrospinning is employed to prepare composite membranes of polyvinylchloride (PVC) embedded with nanocrystals of post-metalated metal organic frameworks (MOFs), UiO-66(COOH)₂-Ag, and ZIF-8-Ag. The composites were fully characterized using scanning electron microscopy (SEM), powder X-ray diffraction (PXRD), thermoGravimetric analysis (TGA), porosity analysis, and water contact angle measurement (WCA). The incorporation of the MOFs nanocrystals within the nanofibrous PVC membranes by electrospinning resulted in the formation of a highly stable MOFs-membrane composite with a larger fiber diameter and greater average pore size compared to PVC. The antibacterial properties of the obtained membranes were investigated as a function of MOF-Ag loading. It showed an improved antibacterial activity (up to 95% inhibition) with the increased MOF-Ag loading when the silver concentration was kept constant which supports a contact-based inhibition. Those findings ensure that such membranes can act as a potential antibacterial air filters due to their nature.

Keywords: Metal Organic frameworks, Composite Membranes, Antibacterial, Electrospinning.

TABLE OF CONTENTS

ACKNOWLEDGEMENTS	1
ABSTRACT.....	2
ILLUSTRATIONS.....	5
TABLES	6
ABBREVIATIONS.....	7
INTRODUCTION.....	8
LITERATURE REVIEW.....	10
A. Nanofibrous Air Filters	12
EXPERIMENTAL	15
A. Materials and Chemicals.....	15
B. MOFs Preparation.....	15
1. Synthesis of UiO-66(COOH) ₂	15
2. Synthesis of UiO-66(COOH) ₂ -Ag.....	16
3. Synthesis of ZIF-8	16
4. Synthesis of ZIF-8-Ag	17
C. Polymeric solution preparation.....	17
D. Nano-fibrous membrane Fabrication:	18
E. Membrane Characterization:	20
F. Anti-Bacterial properties tests:.....	22

RESULTS & DISCUSSION	24
A. MOFs Properties	24
B. Membrane Characterisation	26
1. Scanning Electron Microscope (SEM) and morphology	26
2. Fiber diameter analysis	27
3. TGA analysis	28
4. Pore size and Porosity	29
5. Water Contact Angle and Liquid Entry Pressure Analysis	31
6. Silver loading by Atomic Absorption and TGA.....	33
C. Anti-bacterial Properties	35
CONCLUSIONS AND PERSPECTIVES.....	41
REFERENCES.....	43

ILLUSTRATIONS

Figure

1. Schematic illustration of the metal-organic frameworks (MOFs) molecular structure [37]	11
2. UiO66 (COOH) ₂ and its metalated form [31]	12
3. Electrospinning setup [52]	18
4. (A) PXRD pattern of UiO-66(COOH) ₂ (bottom-black), UiO-66(COOH) ₂ -Ag (top-red), (B) SEM images of UiO-66(COOH) ₂ and UiO-66(COOH) ₂ -Ag. (C) PXRD pattern of ZIF-8 (bottom-black), ZIF-8-Ag (top-red), (D) SEM images of ZIF-8 and ZIF-8-Ag.....	25
5. Thermal Gravimetric analysis (TGA) of the non-metalated and metalated MOFs	25
6. SEM micrographs: Untreated PVC (i, ii); PVC/UiO-66(COOH) ₂ -Ag 5% (A1, A2), 10% (A3,A4), 20% (A5,A6); PVC/ZIF-8-Ag 5% (B1, B2),10% (B3,B4), 20% (B5,B6).....	27
7. Average fiber diameter of the different treated membranes	28
8. TGA of P-U (A), P-Z (B).....	29
9. Pore size distribution of the different membranes.....	30
10. Relationship between pore size distribution and liquid entry pressure (LEP) for all treated membranes.	32
11. PVC-AgNO ₃ (P-A) membranes, (A1, A2) 5%, (A3, A4) 10%, (A5, A6) 20% ..	34
12. TGA for PVC/AgNO ₃ (P-A) membranes.....	35
13. The Relationship between bacterial inhibition (%) and EI for P-U and P-Z of different percentages by weight (5%, 10%, and 20%) at 15 mg/mL of PVC/MOFs-Ag.....	36
14. The difference in bacterial inhibition of P-U and P-Z membranes at 5%, 10%, and 20% MOFs-Ag loading at the same silver concentration.....	38
15. Graphs showing the MIC of P-U (A) and of P-Z (B), and MBC of P-U (C) and of P-Z (D) at 20% MOFs-Ag by weight of PVC.....	39
16. The Relationship between bacterial inhibition and EI for P-A.....	40

TABLES

Table

1. MERV Rating [45]	13
2. Used Electrospinning Parameters	19
3. Water Contact Angle	31
4. Silver (Ag) loading percentage in the loaded samples:	33

ABBREVIATIONS

ES: Electrospinning	Electrospinning
High Efficiency Particulate Air: HEPA	HEPA
Metal Organic Frameworks: MOFs	MOFs
Carboxyl functionalized Zirconium 1,4-dicarboxybenzene MOF ²² : UiO-66(COOH) ₂	UiO-66(COOH) ₂
2-Methylimidazole zinc salt: ZIF-8	ZIF-8
Minimum inhibitory concentrations (MICs)	MIC
Minimum Bactericidal Concentration (MBC)	MBC

CHAPTER I

INTRODUCTION

Due to the industrial and technological revolutions and the excessive use of fossil fuel in addition to the increasing need for energy, pollution and contamination of the atmosphere has increased[1]. In addition, it is proven that many indoor materials and house products emit volatile organic compounds that are harmful for our health[2]. Additionally, outbreaks of communicable diseases have existed ever since the hunter-gatherer days of humankind. Organisms like bacteria, viruses, fungi, and parasites are the major causes of infectious diseases in humans as they lead to nearly 1.5 billion total disability-adjusted life years (DALYs) each year[3]. Moreover, the continuous evolution of these microbial organisms due to mutations and strain reassortment has made some vaccines and antibiotics limited in their use [4]. The effects of outbreaks such that of the COVID-19 pandemic on the health of every individual worldwide were nothing short than devastating[5]. For this reason, clean air has become one of the most important targets for humans nowadays and several approaches have been used to prevent further spreading of any diseases or even to protect humans from harmful dust and particulate matters (PM) that can affect their respiratory system[6, 7]. It starts on the individual level by wearing face masks, all the way to create a clean filtered air inside and outside living places such as vehicles or buildings of all kinds[7].

In order to create a clean environment inside closed spaces, HVAC systems are needed. Those systems utilize filters to capture unwanted particulate matter or microorganisms from air[8, 9]. Air filters are divided into 4 main types depending on the efficiency: pre filter which is of low efficiency, medium filter (medium efficiency), high efficiency particulate air (HEPA) filter and ultra-low particulate air (ULPA) filter[10].

However, Air filters can be contaminated, and many studies showed that the contamination of air filters will lead to a big decrease in the efficiency and quality of the filtered air along with increase in energy consumption [11-13]. Accordingly, a pressing need for membranes and filters that exhibit antibacterial/antifungal properties is rising[14].

One of the most promising methods to produce porous membranes that can act as a high efficiency filters is Electrospinning (ES). Using this method, filters can be produced under the effect of high voltage using a chosen polymeric solution[15]. This process is suitable for producing selective nanofibrous filters since it is possible to tune and control the fiber diameter to have a desirable pore size[16]. Additionally, nanoparticles like metal organic frameworks (MOFs) can be added for the solution so that some extra properties for the membrane can be added such as antibacterial properties [17, 18]. Accordingly, this project intends to use electrospinning as a method of producing polymer/MOFs fibrous membranes by the means of altering the polymeric solution used in this process using silver post metalated MOFs as nanoparticle additives to add antibacterial properties to the produced membrane.

CHAPTER II

LITERATURE REVIEW

As a response to outbreaks, there is a pressing need to search for new ways not only to protect humans from airborne pathogens that are highly transmissible [19]. With even more highly contagious viral strains taking over multiple countries over the past two years[20], the main goal has been mainly to decrease viral spreading by protecting our respiratory systems from infection. The best rapid response in defense to airborne pathogens is the usage of personal protective equipment (PPE), especially surgical face masks to limit means of infection [4]. Furthermore, although the use of face masks has been shown to decrease the risk of bacterial or viral shedding [21, 22], their improper use has been associated with jeopardizing their protective effect and even increasing the risk of secondary transmission and contamination [23, 24]. In addition, several concerns have been raised regarding the survivability of microorganisms on the surface of face masks and thus re-aerosolization of settled particles [25, 26], as well as concerns surrounding the waste mask burden and subsequent fomite transmission [27, 28]. Thus, there is a need to produce masks that are more durable and elicit an antibacterial activity. Various strategies have been previously explored to increase the durability of face masks and their reusability and their antimicrobial activity by using different polymers and incorporating different biocidal agents like Ag nanoparticles, Cu nanoparticles, or reactive oxygen species [5]. Metal-organic frameworks (MOFs) are a hybrid of organic-inorganic porous crystalline materials made up of metal clusters linked together by organic bridging linkers with high porosity and surface area as can be seen in **Figure 1** [29]. MOFs have emerged as a promising material with antimicrobial activity due to their high surface area, porosity,

and the ease of their modification with bactericidal materials such as reactive oxygen species generating materials and silver nanoparticles [30, 31]. Therefore, different variations of MOFs such as zeolite imidazolate framework-8 (ZIF-8) have been incorporated into face masks and have shown to have antibacterial activity against *S. aureus* and were efficient in protecting against COVID-19 [32]. Silver has been known for its effectiveness against a wide range of microbes including gram-negative and gram-positive bacteria [33]. Although the antibacterial mechanism of silver is still yet to be entirely clarified [34], various mechanisms of action have been proposed: silver ions can disrupt bacterial cell walls and cytoplasmic membranes, denature bacterial ribosomes, interfere in bacterial DNA replication, perforate and disrupt membrane by the generation of reactive oxygen species [35, 36]. Although silver has grown a lot of popularity in the biomedical sciences, however, there still remains an issue of regulating silver release in concentrations that are safe for humans remains an area of extensive research.

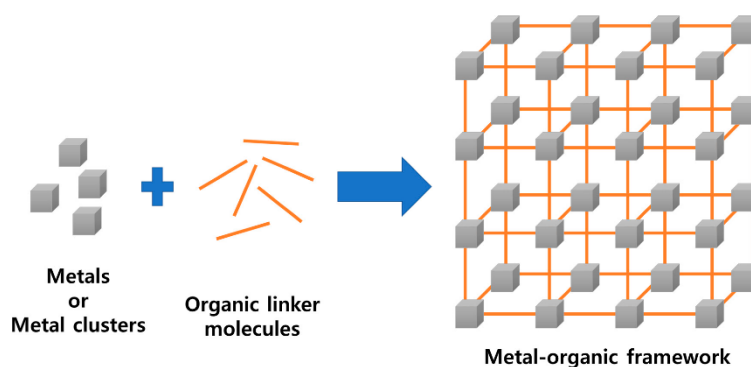


Figure 1 Schematic illustration of the metal-organic frameworks (MOFs) molecular structure [37]

Recently, as mentioned before electrospinning has gained a lot of recognition because of its ability to be used in synthesizing polymeric nano-fibrous materials through the application of a high electrical voltage on a polymer solution [38]. Through this process, it is possible to synthesize nanofibers of various forms and sizes such as membranes,

which have the potential to be used in facemasks. Electrospun nanofiber membranes are promising alternative candidates for acting as facemasks because of their small pore size which allows filtration of particles and infectious agents, their ability to be reused when appropriate disinfection methods are used, and their big surface area and flexibility which allow better capture of air particles [38, 39]. Previously, synthesized post-metalated zirconium-based MOFs using silver nitrate have been established as seen in **Figure 2**. The bactericidal activity of these synthesized silver-based MOFs was evaluated and shown to have good potency with a calculated MIC and MBC of 6.5 $\mu\text{g/mL}$ of silver content [31].

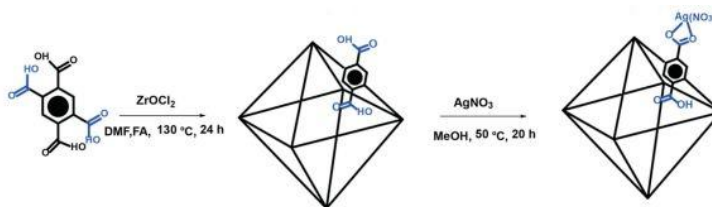


Figure 2 UIO66 (COOH)₂ and its metalated form [31]

A. Nanofibrous Air Filters

The efficiency and filtration ability of conventional air filters is relatively low due to high fiber diameter that leads to high pore size distribution. Accordingly, many attempts have been done to produce nanofibrous membranes of small fiber diameter to act as filters to remove particulate matter from air. For example, polyamide nanofibrous air filters have been synthesized by electrospinning and showed a high efficiency and high thermal stability in removal of $\text{PM}_{2.5}$ [40, 41]. In another study, polyurethane was used to produce hybrid nanofiber/Nets Air filters that exhibit an efficiency of 99% for $\text{PM}_{1-0.5}$ removal [42]. However in ordinary filters, a possible bacterial and fungal colonization can take place even in hospitals as Simmons et al showed in their study [43].

And here comes the importance of having filters that are both highly efficient and antibacterial/fungal at the same time to prevent allergic respiratory diseases and improve air quality[44]. The American Society of Heating, Refrigerating, and Air Conditioning Engineers (ASHRAE)[45], have developed a rating or benchmarking of filters and it is called Minimum Efficiency Reporting Values, or MERVs the values of MERV are shown in table 1. According to the United States Department of Energy, HEPA filters are a mechanical type ‘High Efficiency Particulate Air’ filters. In theory, HEPA filters should be able to remove up to 0.3 μm of airborne particulate matter from air such as dust, pollen and bacteria with efficiency of 99.97% [46].

Table 1 MERV Rating [46]

MERV Rating	Average Particle Size Efficiency in Microns
1-4	3.0 - 10.0 less than 20%
6	3.0 - 10.0 49.9%
8	3.0 - 10.0 84.9%
10	1.0 - 3.0 50% - 64.9%, 3.0 - 10.0 85% or greater
12	1.0 - 3.0 80% - 89.9%, 3.0 - 10.0 90% or greater
14	0.3 - 1.0 75% - 84%, 1.0 - 3.0 90% or greater
16	0.3 - 1.0 75% or greater
High efficiency Particulate Air filter HEPA*	99.97% of particles in the 0.3-micron range Particles that are larger or smaller than 0.3 microns are captured with a greater than 99.97% efficiency

Herein, this work aims to develop a new prototype of nanofibrous antibacterial membranes that can reach MERV rating of 14 or above reaching a HEPA filters level by synthesizing highly stable electrospun polyvinylchloride (PVC) membranes combined with the long-term persistence and thermal stability of $\text{UiO-66}(\text{COOH})_2$ and ZIF-8 post-metalated with silver **Figure 3**. As a proof of concept, the bactericidal activity of these membranes is evaluated against *Escherichia coli* in which the membranes showed good potency and bacterial inhibitory properties.

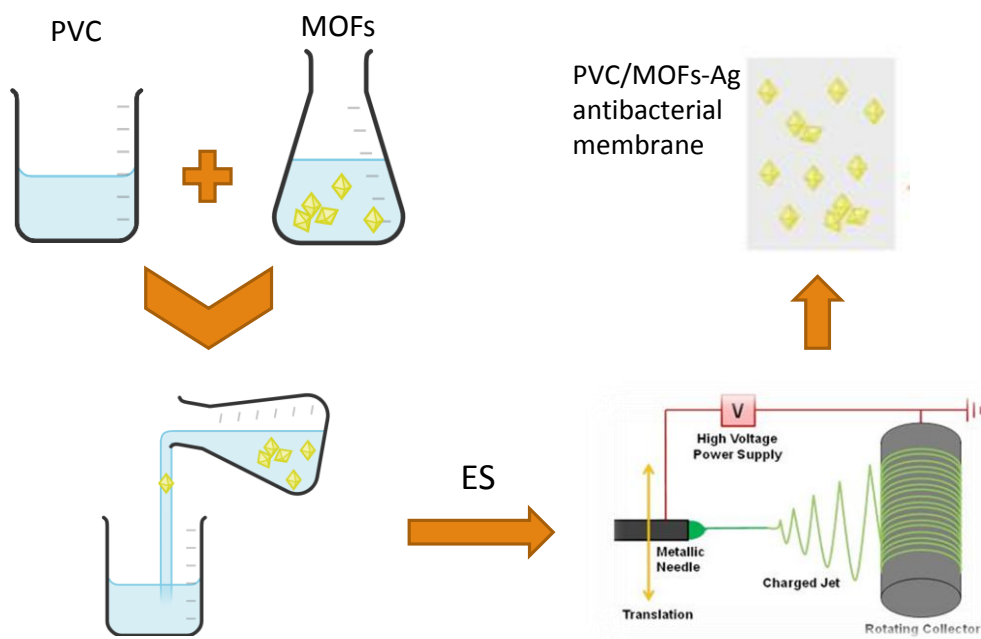


Figure 3 schematic illustration of PVC/MOFs-Ag production.

CHAPTER III EXPERIMENTAL

A. Materials and Chemicals

All chemical reagents and solvents used throughout this work were commercially supplied and utilized without further purification. *N,N*-Dimethylformamide (DMF) (purity $\geq 99.8\%$), Tetrahydrofuran (THF) with $\geq 99.8\%$ purity, Methanol (ACS reagent, $>99.8\%$), Polyvinyl chloride (PVC) with an average molecular weight of 80,000 g/mol and a density of 1.4 g/mL at 25°C, solid silver nitrate (AgNO_3 , 99.8%), Zirconyl chloride octahydrate ($\text{ZrOCl}_2 \cdot 8\text{H}_2\text{O}$), Zinc chloride (ZnCl_2), 1,2,4,5-benzenetetracarboxylic acid ($\text{C}_{10}\text{H}_6\text{O}_8$), 2-methylimidazole ($\text{C}_4\text{H}_6\text{N}_2$), formic acid (ACS reagent, 88-91%), and Luria Bertani (LB) Broth were all purchased from Sigma Aldrich. Mueller Hinton Broth was acquired from Fischer Scientific. Commercial polyester screen fabric with an average pore diameter of 350 μm and a thickness of $215 \pm 2 \mu\text{m}$ was used to cover the cylindrical collector ($D = 10 \text{ cm}$) of the electrospinning machine.

B. MOFs Preparation

1. Synthesis of $\text{UiO-66}(\text{COOH})_2$

$\text{UiO-66}(\text{COOH})_2$ was prepared via a solvothermal method by a synthesis route previously reported in the literature[31]. Briefly, an equimolar amount of Zirconyl chloride octahydrate (0.185 mmol, 59.6 mg) and 1,2,4,5-benzenetetracarboxylic acid (0.85 mmol, 47.1 mg) were dissolved in a 20 mL scintillation vial containing 4 mL of DMF and 4 mL of formic acid modulator. The mixture was then homogenized by sonication and placed in a preheated oven for 5 hours at a temperature of 130 °C. The resulting white $\text{UiO-66}(\text{COOH})_2$ particles were washed with DMF for three consecutive

days, activated by solvent exchange with ethanol for another three days, and finally dried under vacuum for 12 hours at 80 °C.

2. *Synthesis of UiO-66(COOH)₂-Ag*

The prepared UiO-66(COOH)₂ (20 mg) was added to a silver solution containing 40 mg of silver nitrate (AgNO₃) dissolved in 10 mL of methanol. The mixture was then stirred and heated on a hot plate for 20 hours at a temperature of 50 °C to allow for the incorporation of silver into the framework. The resulting brown crystalline powder was collected by centrifugation, washed with DMF and methanol for two consecutive days each, and finally dried under vacuum at 80 °C for 12 hours[31].

3. *Synthesis of ZIF-8*

ZIF-8 was prepared via a reaction-diffusion process by diffusion of a 2-methylimidazolate-based solution into an agar gel matrix containing zinc metal cations[47]. In brief, the inner portion was first prepared by dissolving 136 mg of zinc chloride (50 mM) in a 1:1 mixture of DMF and water followed by the addition of 1% (w/w) of bacteriological agar powder to the mixture. The resulting solution was then heated and stirred on a hot plate to allow for the complete dissolution of the agar gel and finally transferred into a Pyrex tube filling it to two-thirds. After complete gelation of the agar gel, the outer portion was prepared by dissolving 247 mg of 2-methylimidazolate (500 mM) in a 1:1 mixture of water and DMF. The resulting solution was then poured on top of the inner electrolyte filling the rest of the Pyrex tube, covered with parafilm, and left on the bench for a few days to allow for the reaction-diffusion process and formation of the white precipitate front to take place. The precipitation regions of ZIF-8 were

thereafter extracted, washed with DMF to dissolve the agar gel, and later activated by solvent exchange with methanol. Finally, the particles were collected by centrifugation and dried under vacuum for 12 hours at 100 °C.

4. Synthesis of ZIF-8-Ag

ZIF-8-Ag was prepared by introducing silver precursors to ZIF-8 followed by reduction[48]. In brief, 100 mg of ZIF-8 were added to a silver solution containing 17 mg of silver nitrate (AgNO_3) dissolved in 4 mL of DI. The resulting mixture was first sonicated and later stirred on a hot plate for 12 hours at room temperature. ZIF-8 suspension was then collected by centrifugation and dried under dynamic vacuum at 80°C for 12 hours. The light-gray crystalline powder was thereafter soaked in a water solution containing 50 mg of NaBH_4 reducing agent. The mixture was then stirred for 30 mins resulting in the formation of a dark gray powder corresponding to the ZIF-8-Ag. Finally, the resulting product was washed with methanol, collected via centrifugation, and dried under vacuum for 12 hours at 80 °C.

C. Polymeric solution preparation

Normal-PVC solution (16%wt) is prepared by adding PVC powder to a mixture 10:5 of DMF: THF (vol/vol).The mixture was stirred at room temperature for approximately 12 h at an apparent speed of 600 rpm for complete dissolution. Before electrospinning, the polymeric solution was allowed to rest to remove entrapped air bubbles.

Preparation of PVC/MOFs solution: PVC was dissolved using 2/3 of the solvent-mix volume as mentioned above. The other 1/3 was used to disperse the MOFs of

different percentages (5, 10, 20)% wt/wt of the polymer using sonication for 30 mins, finally the two solutions were mixed and stirred for another 30 mins.

For comparative reasons PVC/AgNO₃ solution was also prepared by dissolving the desired percentages (5, 10, and 20) % wt/wt of AgNO₃ salt in 2ml of the DMF: THF mixture then adding it into the completely dissolved PVC solution.

D. Nano-fibrous membrane Fabrication:

Producing nano-fibrous thermoplastic polymeric membranes using electrospinning can be quite challenging, especially upon adding other materials to the main solution. Many parameters can play an important role in determining the morphology and the stability of the production. The synthesis of these nano-fibrous membranes relies on the solution concentration, viscosity, conductivity, type of solvent, and the electrospinning conditions which include the applied voltage, pumping flow rate, and the tip to collector distance (TCD) [49-51]. The Electrospinning setup is shown in **Figure 4**.

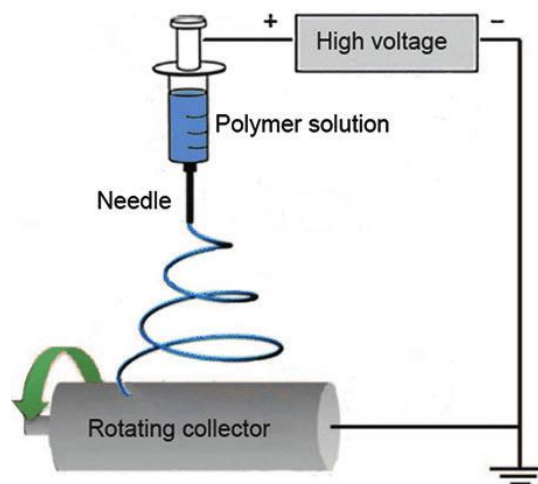


Figure 4 Electrospinning setup [52]

The membranes are fabricated using lab-scale electrospinning (ES) machine (Fluidnatek by Biolnacia). The drum collector (D = 10 cm) was first covered with a

polyester fabric. A 20 mL plastic syringe was then filled with the polymeric solution, which was then fed to the nozzle at a flow rate of 3 mL/h using a syringe pump. It is important to note that the addition of either the UiO-66(COOH)₂-Ag, ZIF-8-Ag or AgNO₃ to the main polymer solution changes its conductivity and viscosity. Therefore, the ES parameters have to be modified to obtain the best stable polymer jet possible. The electrospinning conditions (**Table 2**) used to produce the nano-fibrous membranes were taken after a sequence of selection and optimization steps. In the case of PVC/ZIF-8-Ag, the same ES conditions as untreated PVC were employed without any changes. However, for the PVC/UiO-66(COOH)₂-Ag and PVC/AgNO₃, different voltages were used. All membranes were collected after 2.5 hours of electrospinning. Three membrane systems are synthesized in this work, PVC/ZIF-8-Ag (P-Z), PVC/UiO-66(COOH)₂-Ag (P-U), and a reference membrane PVC/AgNO₃ (P-A). Each system includes three different silver-metalated MOFs loading percentages (5, 10, and 20%) in addition to the untreated PVC membrane, which adds up to 10 different membranes in total (**Table 2**).

Table 2 Used Electrospinning Parameters

	% loading	Voltage (KV)	Flow rate (ml/hr)	TCD	RPM
Untreated PVC	0	18	3	15	600
PVC/AgNO ₃	5	25	3	15	600
	10	25	3	15	600
	20	25	3	20	600
PVC/Zif8-Ag	5	18	3	15	600
	10	18	3	15	600
	20	18	3	15	600
PVC/UIO(COOH) ₂ -Ag	5	14	3	15	600
	10	14	3	15	600
	20	14	3	15	600

E. Membrane Characterization:

A thickness gauge (MP-1, Brunswick Instrument, and UK) with a probe tip and floating stand anvil was used for measuring the thickness of produced membranes. The measurements were collected according to ASTM-D1777 by applying a pressure of (~1464 Pa) on the objects.

Scanning electron microscope (SEM MIRA 3 LMU Tescan, Czech Republic) with an In-Beam detector was used to monitor the membrane's morphology and to measure its fiber diameter. Before SEM, The samples taken from each membrane were gold coated with a thin layer (10nm) using a (Q150 T) turbo pumped sputter coater (Quorum Technologies). The working distance between the lenses and the sample varied between 8 and 24 mm, with an acceleration voltage of 5 kV. The in-beam detector was used at a magnification range of 20–50 K. The SEM micrographs of the membranes were analyzed using the MIRA image processing software to measure the average fiber diameter.

The water contact angle formed on the hydrophobic porous electrospun membranes surface was measured using an optical tensiometer (OCA 15EC, Data Physics, Germany). The droplets were ranged from (1-5 μ l). The contact angle is defined as the angle formed between the liquid–vapor interface and the liquid–solid interface.

Capillary flow Porometer (CFP-1100AH, PMI, NY, USA) instrument was used to estimate the pore size distribution within the fabricated membranes. Briefly, a membrane was inserted into the membrane cell holder and using Galwick (of low surface tension 15.9 mN/m) as the wetting agent. The flow of saturated air (Q), passing through the membrane was steadily increased, and the resultant pressure difference (ΔP) was

measured. The pore size distribution was then calculated based on the measured flow rate (Q) as a function of pressure difference (ΔP).

Liquid Entry Pressure (LEP) of the hydrophobic porous membranes was also measured using the capillary flow Porometer. For this measurement, a layer of DI water was added on top of the membrane to measure maximum hydrostatic pressure that a membrane can tolerate before failing (leaking).

For the membrane's thermal analysis, ThermoGravimetric analysis (TGA) Q500 machine was used. The temperature range was set between 30-1000°C with step of 10K/min.

The amount of silver incorporated in the frameworks was determined by iCE 3000 series atomic absorption spectrophotometer. In brief, the MOF-loaded membranes were first decomposed in a small quantity of DMF. The resulting loaded MOF powders were washed with ethanol three times and dried in a vacuum oven overnight at 80°C.

0.6 mg of each Ag-loaded MOF was transferred to a falcon tube containing 200 μ l of an Aqua Regia solution consisting of a 1:3 ratio of Nitric acid (HNO_3 , 65%) and hydrochloric acid (HCl , 37%) respectively. The mixture was then sonicated for few minutes followed by the addition of 200 μ l of hydrofluoric acid (HF , 50%) to allow for the degradation of the frameworks in addition to 10 mL of deionized water to dilute the solution.

Silver weight % was determined by flame atomic absorption spectroscopy (AAS) using an air-acetylene flame as a fuel source and was calculated using the below formula:

$$\% \text{ Ag Weight} = \frac{C \times V}{m} \times 100$$

Where “C” is the silver’s concentration in the MOF sample in ppm (mg/L) determined via AAS, “V” is the total volume of the solution in L, and “m” is the mass of the MOF sample used in mg.

F. Anti-Bacterial properties tests:

The antibacterial activity of post-metalated MOFs on PVC surfaces was tested against gram-negative *E. coli* (ATCC 25922). The minimum inhibitory concentration (MIC) and the minimum bactericidal concentration (MBC) values against *E. coli* were calculated according to The Clinical & Laboratory Standards Institute (CLSI) protocols and as described in more detail by Wiegand *et al.*[53] A few colonies of *E. coli* were scraped from the surface of a freshly prepared plate and inoculated into 3 mL of LB broth solution and incubated overnight at 37°C with constant shaking at 150 rpm. The overnight culture was then centrifuged and the supernatant was then discarded. PBS solution (5 mL) was added to the formed pellet. The suspension was then vortexed and 100 µL was transferred to 3 mL of Mueller-Hinton Broth (MHB) and incubated for 3-4 hours to achieve a solution of bacterial cells in the lag phase. The absorbance of the sample was assessed using NanoDrop 2000c spectrophotometer (Thermo Fisher Scientific) and diluted to be in the range of the 0.5 McFarland standard (OD₆₀₀ nm between 0.08-0.013). The obtained suspension was then diluted to reach an *E. coli* final concentration of 1×10^5 and 1×10^6 CFU/mL.

PVC containing different loading percentages of silver metalated MOFs were then weighed, cut into small pieces using sterile forceps, and then sterilized by UV light under a biosafety cabinet hood for 15 minutes. The membranes were then suspended in MHB at a set concentration and then incubated with *E. coli* for 18 hours at 37 °C with

shaking at 200 rpm. The turbidity of the obtained samples was then assessed visually and the OD₆₀₀ was measured using a NanoDrop 2000c spectrophotometer to determine the MICs of our samples. Percentage bacterial inhibition was calculated through the following formula:

$$\text{Inhibition \%} = 100\% - \left(\frac{\text{Absorbance of sample}}{\text{Absorbance of positive control}} \right) \times 100$$

For comparison purposes, we will be reporting an effective inhibition factor (EI) calculated from the ratio of the inhibition percentage to the measured silver content in $\mu\text{g/mL}$.

$$EI = \frac{\text{Inhibition \%}}{[Ag] \mu\text{g/mL}}$$

When comparing EIs of different samples, we still ensure that the silver concentrations are close in value.

As for the MBC, which is defined as the lowest concentration of silver that resulted in 99.9 % of bacterial killing, it was determined by taking 100 μL aliquots from the growth tubes and plating them on Luria Bertani (LB) agar plates. The LB agar plates were then incubated at 37°C for 18 hours and then visually inspected for colony growth.

CHAPTER IV RESULTS & DISCUSSION

A. MOFs Properties

The powder X-ray diffraction patterns of the MOFs and their metalated forms were well resolved and in good agreement with the simulated ones, confirming the high crystallinity and the phase purity of the produced samples (**Figure 5A and 2-C**). Furthermore, no additional peaks could be observed for silver-based crystalline species due to the low loading and high dispersity on the UiO-66(COOH)₂ and ZIF-8 crystals. As can be seen from the SEM images (**Figure 5-B**), the crystals of UiO-66(COOH)₂ (white) and UiO-66(COOH)₂-Ag (yellow) were of octahedral shapes with an average particle size of $0.5 \pm 0.1 \mu\text{m}$, while ZIF-8 (white) and ZIF-8-Ag (greenish-gray) samples exhibited a rhombic dodecahedron morphology and an average size of $3 \pm 1 \mu\text{m}$ (**Figure 5-D**). These data show that the crystalline nature and the morphology of the studied MOFs structures are preserved upon Ag-metalation.

The TGA analysis of the metalated and non-metalated MOFs samples (**Figure 6**) showed that the weight % remaining in both metalated MOFs was higher than that of non-metalated ones. This is due to the presence of silver metal in the samples. However, UiO-66(COOH)₂-Ag decomposes at 380°C which is lower than that of non-metalated UiO-66(COOH)₂ which decomposes at 565°C. This indicates that the thermal stability of UiO-66(COOH)₂-Ag is lower than that of UiO-66(COOH)₂. On the other hand, ZIF-8-Ag is more stable than ZIF-8 at temperatures below 480 °C and of comparable thermal stability at higher temperatures. This implies that silver metalation has decreased the thermal stability of UiO-66(COOH)₂ and increased it for ZIF-8. The silver content in the

metalated-MOFs was estimated using AAS and found to be 8.3 % wt for ZIF-8-Ag and 9.1 % wt for UiO-66(COOH)₂-Ag.

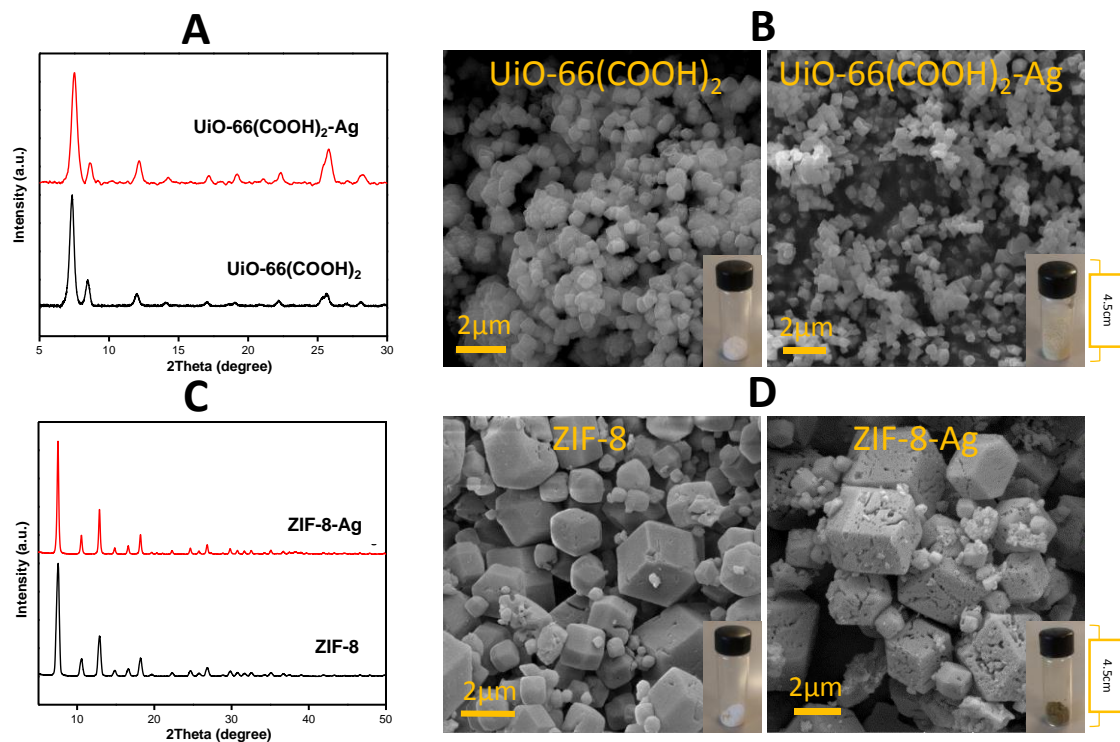


Figure 5 (A) PXRD pattern of UiO-66(COOH)₂ (bottom-black), UiO-66(COOH)₂-Ag (top-red), (B) SEM images of UiO-66(COOH)₂ and UiO-66(COOH)₂-Ag. (C) PXRD pattern of ZIF-8 (bottom-black), ZIF-8-Ag (top-red), (D) SEM images of ZIF-8 and ZIF-8-Ag.

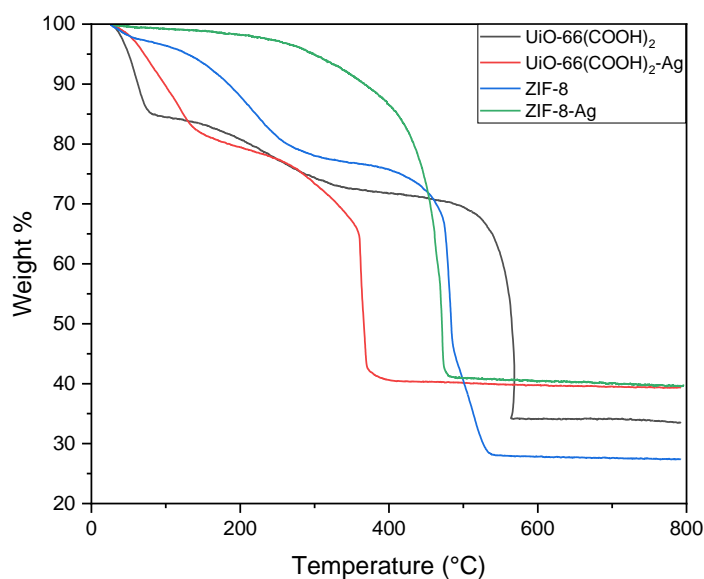


Figure 6 Thermal Gravimetric analysis (TGA) of the non-metalated and metalated MOFs

B. Membrane Characterisation

1. Scanning Electron Microscope (SEM) and morphology

The optical and SEM images of the white untreated PVC membranes produced by electrospinning are shown in (**Figure 7-i, ii**). These PVC membranes displayed smooth continuous fibers with an average diameter of $0.7 \pm 0.3 \mu\text{m}$. Upon addition of the small UiO-66(COOH)₂-Ag crystals to the PVC solution, the morphology of the PVC/MOFs-Ag system became distinguishable from that of pristine PVC as seen in the SEM images (**Figure 7**). In fact, we can clearly visualize embedded MOFs-Ag inside the PVC fibers in the form of clumps and aggregates. The aggregates' size increased to a point where the ES jet was unstable, and the membrane was full of bead-like structures with an average diameter of $15.5 \pm 7.8 \mu\text{m}$ at 20% MOFs-Ag loading (**Figure 7-A5**). Moreover, the presence of the UiO-66(COOH)₂-Ag in the membrane changed its color from white to yellowish which became darker at higher loading percentages (**Figure 7**). Unlike P-U membranes, ZIF-8-Ag crystals in P-Z samples were mostly embedded inside the PVC fibers as shown in the SEM images in **Figure 7-B1 to B6**. This is mainly due to the larger crystal size of the ZIF-8-Ag. It was also observed that the amount of ZIF-8-Ag increased with increasing loading percentage until big bead-like structures were observed at 20% loading with an average diameter of $27.4 \pm 4 \mu\text{m}$ (**Figure 7-B5**). Such beads were not observed in the case of 5% and 10% loadings. The observed color of the membranes was of greenish-gray color, which became more prominent as the percentage (%) of Ag-loading increased (**Figure 7**).

Untreated PVC

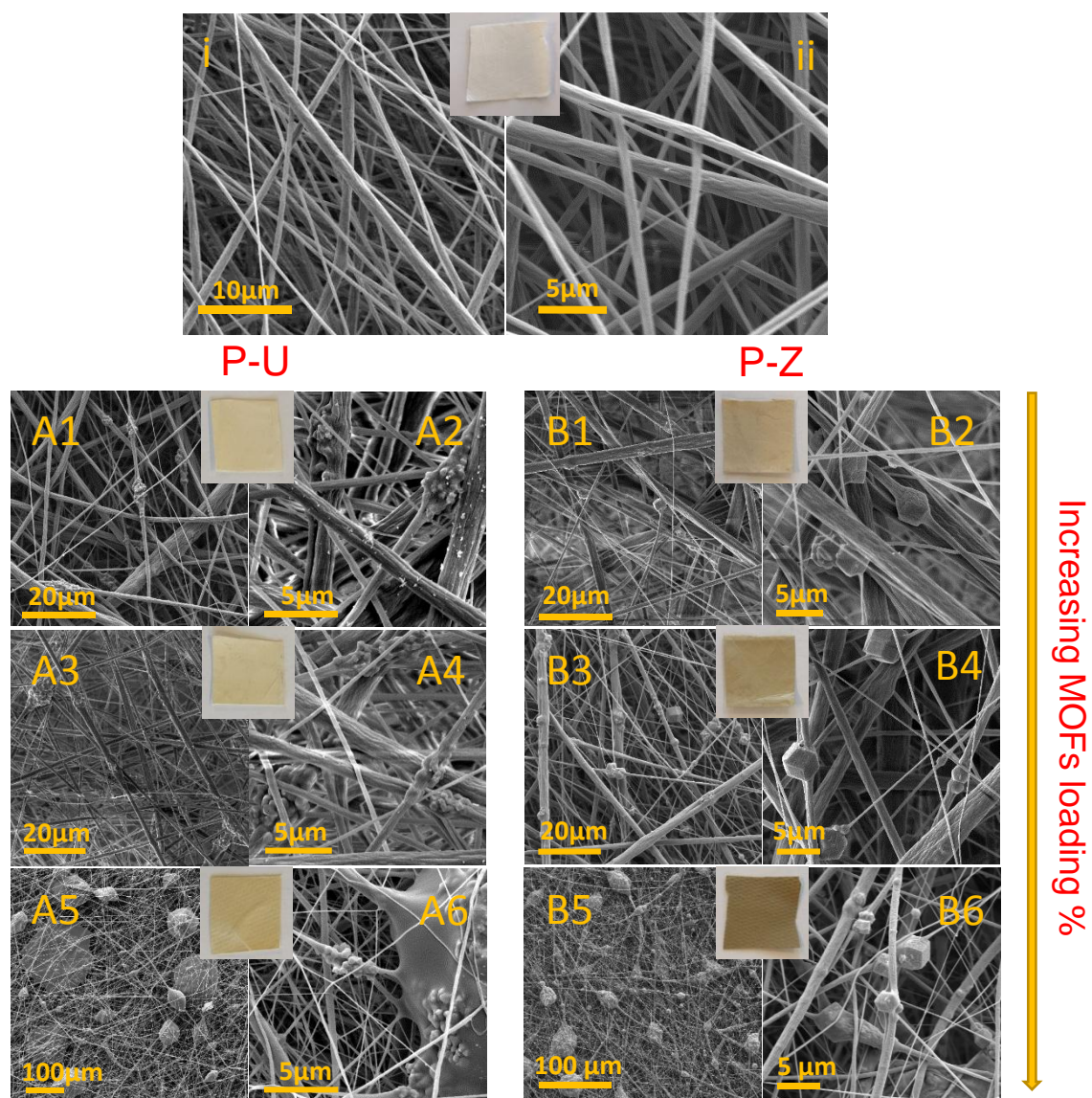


Figure 7. SEM micrographs: Untreated PVC (i, ii); PVC/UiO-66(COOH)₂-Ag 5% (A1, A2), 10% (A3,A4), 20% (A5,A6); PVC/ZIF-8-Ag 5%(B1, B2),10%(B3,B4), 20% (B5,B6).

2. Fiber diameter analysis

The presence of the UiO-66(COOH)₂-Ag increased the fiber diameter by 0.1 μm to be 0.8 μm in the case of 5% and 10% loadings which is considered a minor change whereas in the case of 20% loading the fiber diameter decreased sharply to reach 0.1 μm as seen in (**Figure 8**) for P-U samples. In the case of ZIF-8-Ag (P-Z), at 5% and 10%

loadings, the fiber diameter increases from 0.7 μm (for the untreated PVC) to 1.1 μm and 1 μm , respectively. But in the case of 20% ZIF-8-Ag loading, however, a minor effect ($0.7 \pm 0.4 \mu\text{m}$ to $0.6 \pm 0.6 \mu\text{m}$) on the fiber diameter was observed (**Figure 8**).

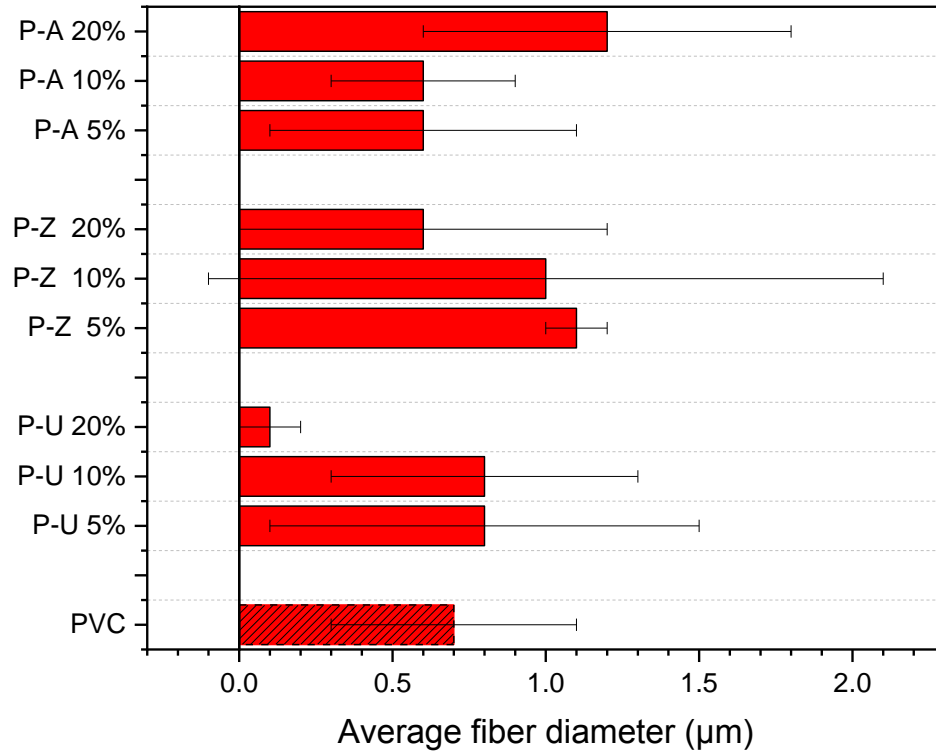


Figure 8 Average fiber diameter of the different treated membranes

3. TGA analysis

The TGA results of the untreated PVC nano-fibrous membrane and the P-U samples are shown in (**Figure 9-A**). We noticed that at 400°C, the remaining weight percentage of untreated PVC was around 38% compared to 44% for P-U at 20% loading. This difference in the weight % loss is due to the presence of silver metalated-MOFs in the membrane.

The addition of ZIF-8-Ag showed a significant impact on the thermal behavior of the treated membrane. As demonstrated in (**Figure 9-B**), all ZIF-8-Ag treated samples (P-Z) were less stable in terms of mass loss as they started rapid sharp degradation at 240

°C compared to untreated PVC which showed a broad rapid degradation starting from 260 °C. Unlike PVC membrane which lost 62% of its original mass at 400 °C, P-Z membranes lost much less reaching around 45% in the case of 20% MOFs-Ag loading. In fact, untreated PVC was completely carbonized at around 600 °C while P-Z (20%) was still holding 30% of its mass, which corresponds to the silver metalated MOFs species.

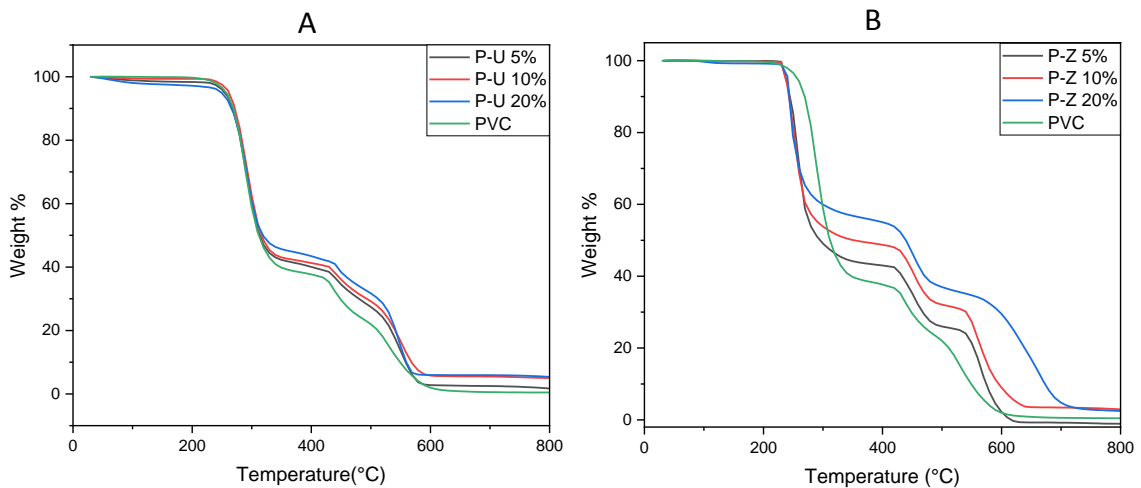


Figure 9 TGA of P-U (A), P-Z (B)

4. Pore size and Porosity

The porosity of nano-fibrous membranes is usually determined by the fiber diameter. When particles were added to the membrane, the porosity and the overall physical and chemical properties of the membrane were affected by the amount and size of the added particles which consequently altered the fiber diameter as well as the fiber stacking. In theory, there is a positive correlation between fiber diameter and pore size such that if the fiber diameter is small, the packing density would be higher and thus the pore size would be smaller [54]. As can be seen in (**Figure 10**), the untreated PVC membrane has an average and maximum pore size of 2.6 μm and 4.6 μm , respectively. With the addition of 5 w% and 10 w% of AgNO_3 , these values remained nearly the same as that of the untreated PVC membrane. However, they were much higher for the 20 w%

P-A. These results are consistent with the fiber diameter results shown above (**Figure 8**). As for P-U and P-Z, the pore size had noticeably changed. Low concentrations of MOFs-Ag (5%) namely both ZIF-8-Ag and UiO-66(COOH)₂-Ag, caused a significant increase in the average and maximum pore size when compared to the untreated PVC. P-U showed a decrease in average and maximum pore size with the increasing MOFs-Ag loading % until it reached 0.5 μm and 4.3 μm respectively at 20% MOFs-Ag loading. This can be explained by the smaller fiber diameter obtained when MOFs-Ag particles coagulate at high loading percentages leading to more stacking and packing density and thus less pore size as was shown previously in the SEM images in **Figure 7** and **Figure 8**. In the case of P-Z, the large crystal size of the MOFs prevented the fibers from agglomeration, which led to a decrease in fiber packing density and consequently an increase in the pore size. The further increase in loading % did not affect the pore size even though the fiber diameter was relatively higher. This is related to the size of the ZIF-8 crystals, which showed minor changes compared to P-U. This indicates that the size of the MOFs-Ag had a significant effect on the pore size of the loaded membranes.

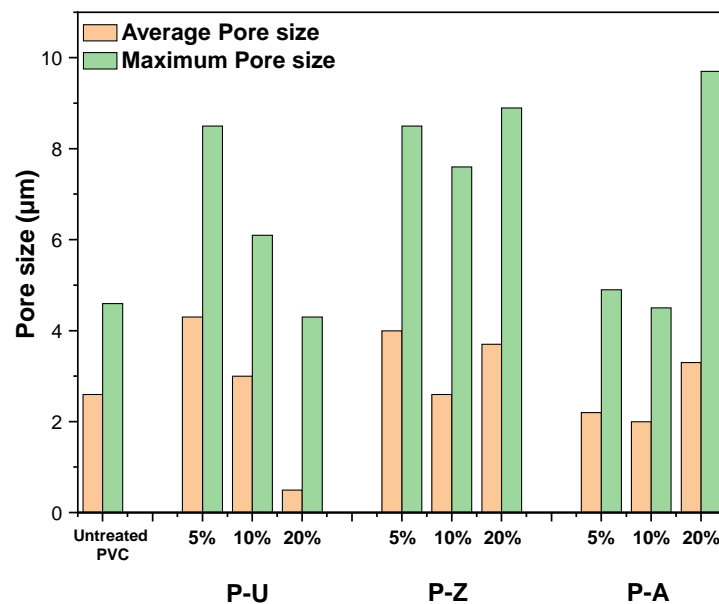



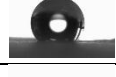
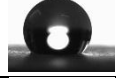
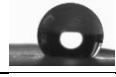
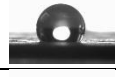
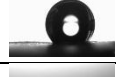



Figure 10 Pore size distribution of the different membranes.

5. Water Contact Angle and Liquid Entry Pressure Analysis

WCA and LEP are very important characteristics that give valuable insight into how the membrane is going to physically interact with polar molecules such as water. **Table 3** shows the Water Contact Angle measurements of all produced membranes in comparison with the untreated PVC. Results show that the obtained membranes are hydrophobic. Moreover, taking into consideration the standard deviation, we can conclude that after introducing MOFs-Ag or AgNO₃, the WCA was not considerably affected, and the membranes kept their water-repelling characteristics. LEP is generally the measure of how much pressure the membrane can handle before failing and it is highly affected by the hydrophobicity and the maximum pore size of the membrane[55]. WCA measurements confirmed that the hydrophobicity was not compromised and accordingly, the main contributor to the change of LEP was the pore size.

Table 3 Water Contact Angle

Membrane	WCA °	
Untreated PVC	135 ±2	
P-U 5%	135 ±2	
P-U 10%	138 ±3	
P-U 20%	136 ±2	
P-Z 5%	133 ±2	
P-Z 10%	133 ±2	
P-Z 20%	128 ±3	
P-A 5%	136 ±2	
P-A 10%	135 ±2	

P-A 20%	130 ±4	
---------	--------	--

Figure 11 summarizes the relation between the measured pore size and LEP upon the addition of different MOFs. LEP increased with the decrease in pore size for P-U and P-A membranes, but slightly increased with the increase in pore size in the case of P-Z treated membranes. Theoretically, the bigger pore size in P-Z membranes results in lower LEP[55]. However, because ZIF-8-Ag crystals are similar in size to the average pore size of the membrane, “pore blockage” would take place, decreasing the pore count of the membrane (which is the actual number of pores present in the sample for a given area) and thus compensating for the high pore size distribution. This ultimately led to comparable LEP to untreated PVC, which could be advantageous in our case as high loading and relatively high LEP are obtained.

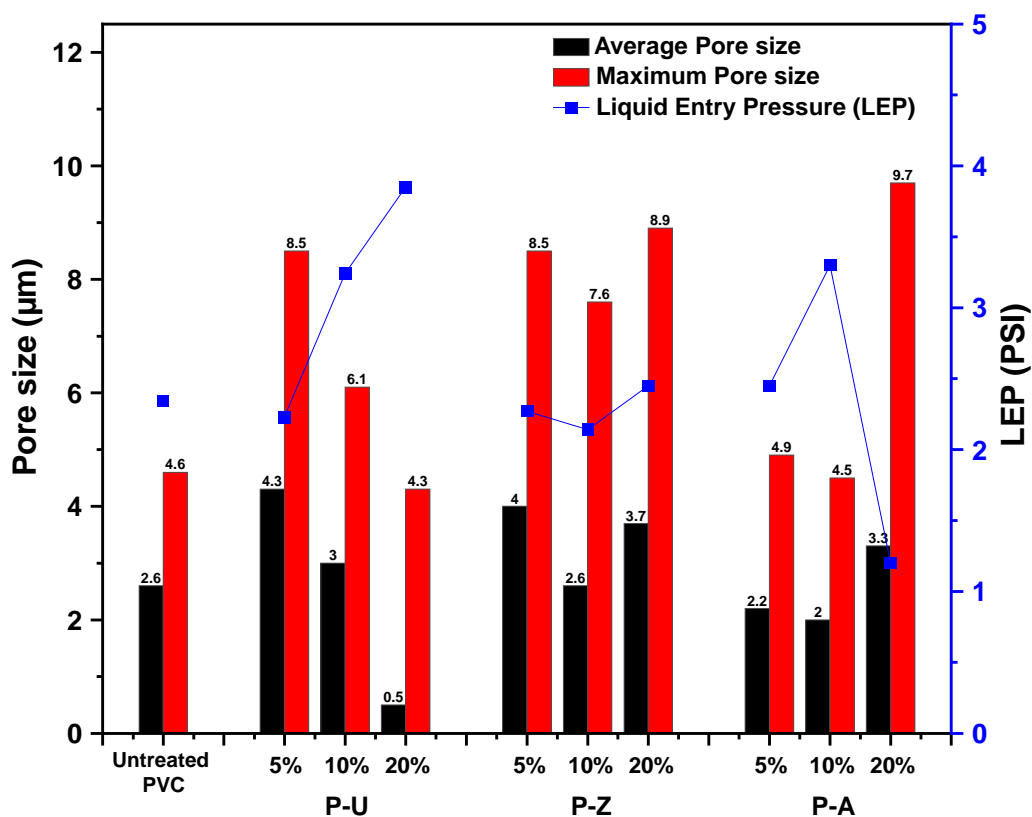


Figure 11 Relationship between pore size distribution and liquid entry pressure (LEP) for all treated membranes.

6. Silver loading by Atomic Absorption and TGA

For the MOFs-Ag loaded membranes, the exact silver loading % was measured using AAS (see the experimental section for more details) while for P-A samples, TGA is employed, according to a protocol mentioned in the Supplementary Information. The results are shown in **Table 4**.

Table 4 Silver (Ag) loading percentage in the loaded samples:

Membrane	Silver loading %	Method used
P-U 5%	0.31%	(AAS)
P-U 10%	0.52%	(AAS)
P-U 20%	1.46%	(AAS)
P-Z 5%	0.26%	(AAS)
P-Z 10%	0.57%	(AAS)
P-Z 20%	0.92%	(AAS)
P-A 5%	1.29%	(TGA)
P-A 10%	4.56%	(TGA)
P-A 20%	7.94%	(TGA)

In order to appraise the role of the MOFs-Ag structure in the fabricated membranes, reference membranes incorporating only AgNO_3 silver salts were synthesized under similar conditions to those employed for P-U and P-Z. SEM images of P-A membranes showed no noticeable effect on the morphology of membranes (**Figure 12-A1, A2**) for 5 % AgNO_3 compared to untreated PVC (**Figure 7-i, ii**). For 10 % (**Figure 12-A3, A4**) and 20 % (**Figure 12-A5, A6**) MOFs-Ag loadings, it was clear from the SEM images that small spherical nanoparticles were located on the surface of the fibers with no change in their overall structure. One thing to note is that there is a small increase in fiber diameter at 5% and 10% of AgNO_3 loading and a very significant decrease at 20% (**Figure 8**). The major change in fiber diameter is related to the change in the conductivity of the solution after the addition of AgNO_3 silver salt. This has been

proven to affect the solution behavior in ES and consequently on the fiber diameter [56-58]. In addition, while the color of the three prepared membranes was white at the very beginning, they turned into brown color due to oxidation of the silver nitrate. The intensity of the color increased with the increase in the loading percentages (**Figure 12**). Also, while the addition of AgNO_3 to PVC had a small impact on the thermal behavior of the membrane at low temperatures ($<310^\circ\text{C}$), it had a noticeable effect at higher temperatures where P-A membranes showed a rapid decrease in mass % starting at 550°C . On the other hand, untreated PVC membranes showed a fast decrease at 440°C and then continued to gradually decrease until the end. It is worth mentioning that above 600°C all the membranes reached a final plateau, and as shown, the higher the % loading, the more mass remained after the process was over (**Figure 13**).

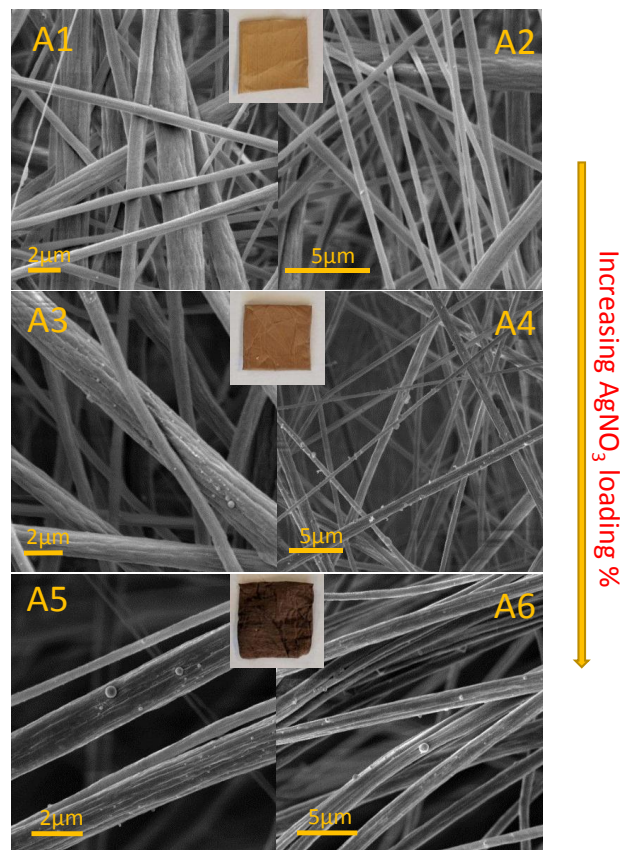


Figure 12 PVC- AgNO_3 (P-A) membranes, (A1, A2) 5%, (A3, A4) 10%, (A5, A6) 20%.

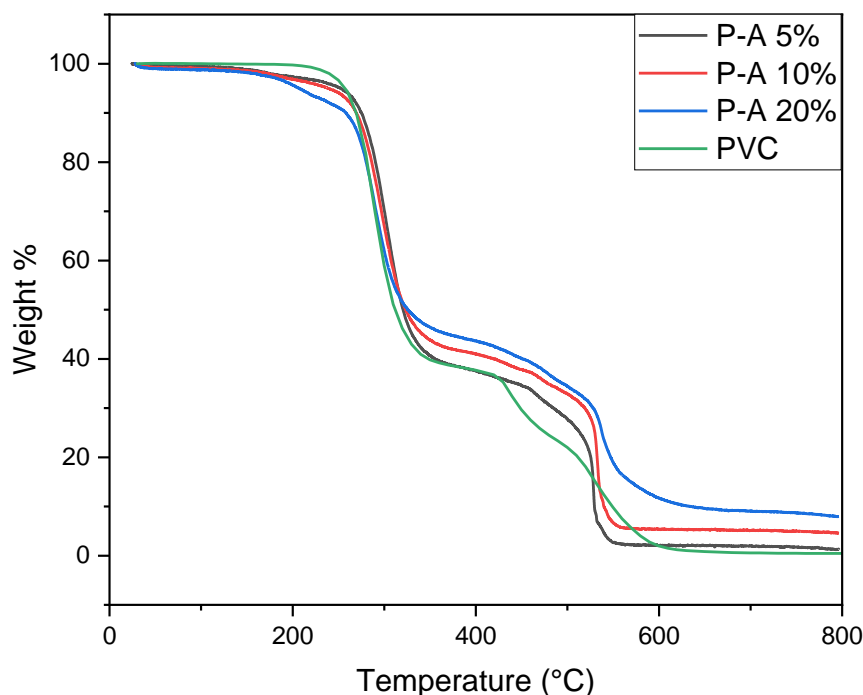


Figure 13 TGA for PVC/AgNO₃ (P-A) membranes.

C. Anti-bacterial Properties

As a proof of concept of the antibacterial activity of prepared electrospun membranes, we tested the growth inhibition and the bactericidal effect of the prepared membranes against *E. coli* at 5%, 10%, and 20% of MOFs-Ag loading in P-U and P-Z systems. The percentage inhibition of *E. coli* is calculated relative to a positive control of 100% bacterial growth in the absence of any membrane after 18 hours of incubation.

At 5% MOFs-Ag loading, the bacterial inhibition of P-Z is 9% with a calculated EI of 0.69 while that of P-U exhibited a much higher inhibition of 32% and an EI= 2 (Figure 14). When the MOFs-Ag loading percentage increased to 10%, both membranes showed an increase in bacterial inhibition to 38% and 50% for P-Z and P-U, respectively. However, when the effective inhibition is calculated, the P-U membranes showed no significant change with an EI of 1.92 while the P-Z effectiveness doubled to reach an EI value of 1.33 (Figure 14). A further increase in the MOFs-Ag loading to 20%, led to an

increase in inhibition to 77% and 95% for P-Z and P-U, respectively. The effective inhibition is calculated to be 1.88 for P-Z and 1.30 for P-U.

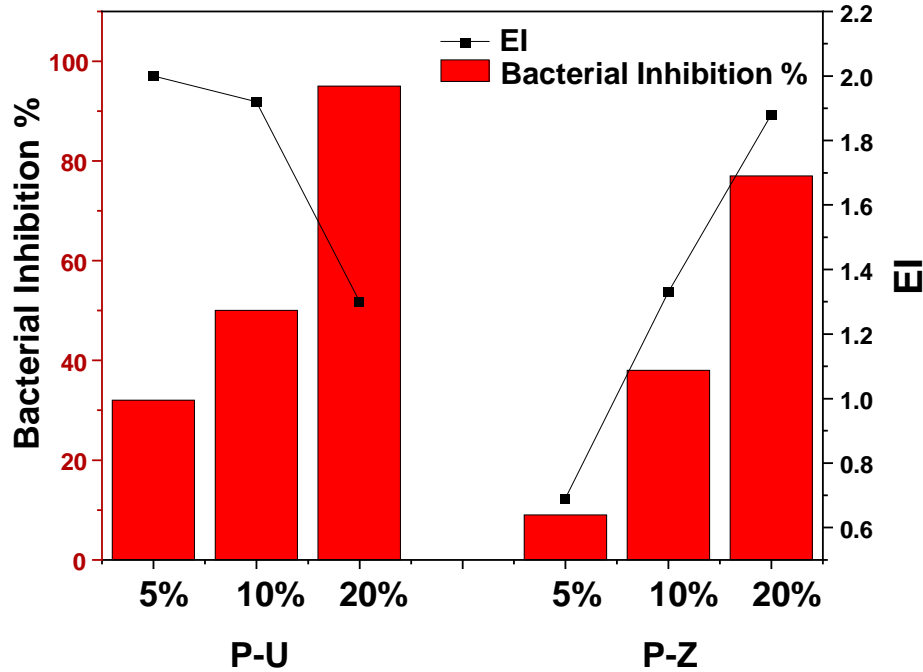


Figure 14 The Relationship between bacterial inhibition (%) and EI for P-U and P-Z of different percentages by weight (5%, 10%, and 20%) at 15 mg/mL of PVC/MOFs-Ag.

It is evident that the increase in surface coverage had a direct effect on the effective inhibition of the PVC/MOFs-Ag membranes. We, therefore, tested the bactericidal effect of PVC/MOFs-Ag membranes at different surface coverages but with similar silver concentrations. As seen in (**Figure 15**), a substantial increase in bacterial inhibition is observed when the MOFs-Ag weight percent increases to 20% in both systems. For instance, when silver concentration is varied between 15 to 17 $\mu\text{g/mL}$ and is tested for P-U at 5, 10, and 20%, the inhibition decreases from 32% to 20% then increases to 62%, respectively. The same trend is observed with the P-Z at 5, 10, and 20% where the inhibition started at 9%, decreased to 4%, and then reached 60%, respectively.

We believe this substantial enhancement in inhibition at 20% weight percent is due to the increase in the local density of the MOFs-Ag particles which supports a contact-base inhibition mechanism versus a slow Ag⁺ release. The higher local concentration might also inhibit the biofilm formation which creates an ideal environment for the bacteria for exponential growth and isolate the micro-organism even under severe antibiotic treatment[59]. While the increase in the antibacterial effect is expected with the increase in silver concentration following the MOFs-Ag loading percent, the effective inhibition factor enhancement is remarkable for the P-Z membranes (**Figure 14**). When looking at the changes in the physical properties of P-Z membranes with increasing the MOFs-Ag loading, an increase in the pore sizes is observed which results in a lower liquid entry pressure (**Figure 11**). Therefore, it is easier for the micro-organism to penetrate the P-Z membranes which lead to better surface contact exposure with the metalated MOFs. This hypothesis is supported by the work of Regiel *et al.* who showed that the dispersion of silver nanoparticles on chitosan films affected the inhibition of biofilm-forming and antibiotic-resistant *Staphylococcus aureus* after short contact times[60]. The high biocidal effect is only achievable upon direct contact between the bacteria and the films and a little to no effect when the contact is eliminated. Direct contact inhibition is also demonstrated by Bondarenko *et al.* who not only showed the extracellular dissolution of silver but also the dissolution taking place at the particle-cell interface which played an essential role in the antibacterial action of AgNPs with bacteria of the highest tendency to attach to nanoparticles surfaces exhibiting the highest sensitivity to all forms of nanoparticle Ag[61].

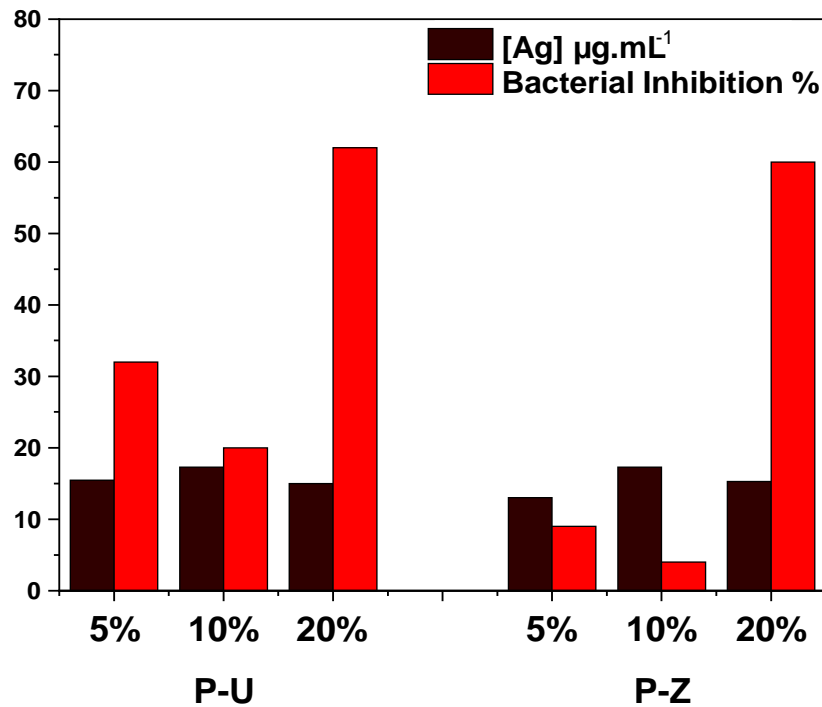


Figure 15 The difference in bacterial inhibition of P-U and P-Z membranes at 5%, 10%, and 20% MOFs-Ag loading at the same silver concentration.

To calculate the MIC and MBC of the 20% modified PVC membranes, the antibacterial activity against *E. coli* was tested at a measured silver concentration between 7 $\mu\text{g/mL}$ and 97 $\mu\text{g/mL}$. The membranes were incubated overnight in freshly prepared bacterial cultures. The results were first assessed visually and then by measuring the optical density to determine the MIC. Serial dilutions from the incubated solutions are plated on agar and then kept at 37°C for 18 hours to determine the MBC concentration. For the P-Z membranes, results showed antibacterial activity with an MIC of 41 $\mu\text{g/mL}$ and an MBC of 54 $\mu\text{g/mL}$ in calculated silver concentration. On the other hand, P-U membrane results showed slightly better antibacterial activity with an MIC of 61 $\mu\text{g/mL}$ and an MBC of 73 $\mu\text{g/mL}$, in calculated silver concentration (**Figure 16**). This observation could be the result of the difference observed in the physical characterization of the composite membranes (e.g. pore size, fiber diameter).

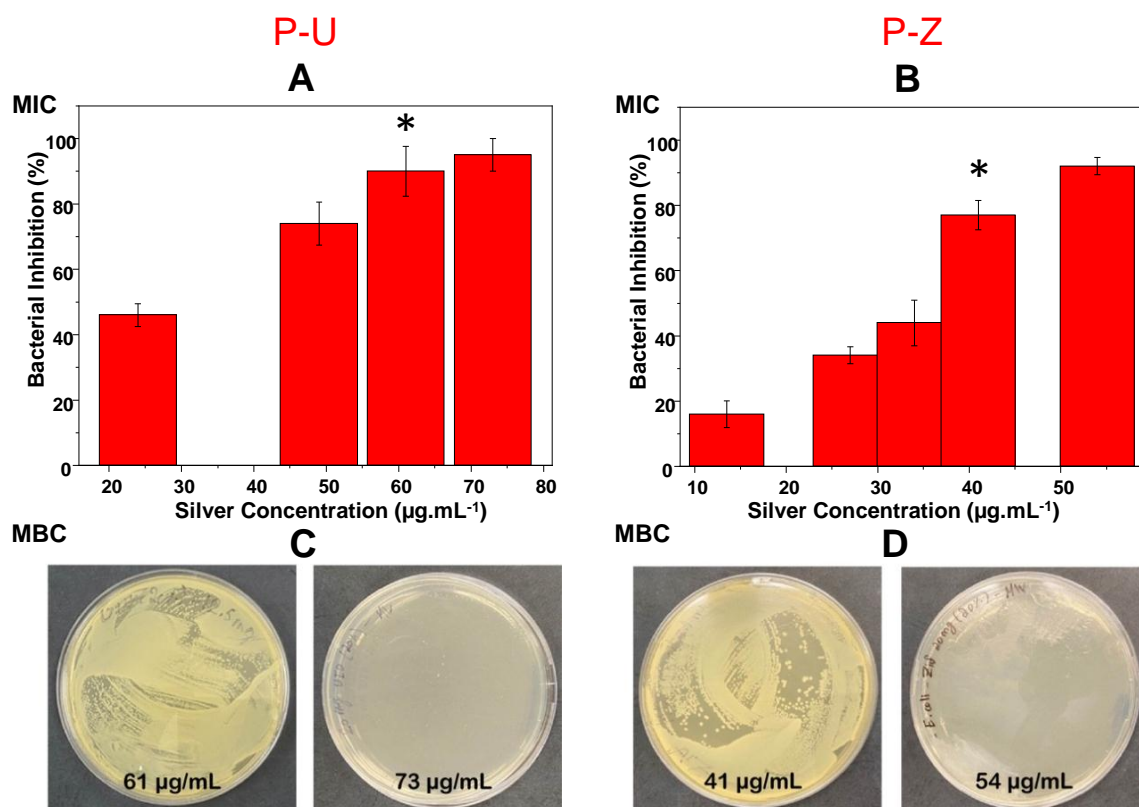


Figure 16 Graphs showing the MIC of P-U (A) and of P-Z (B), and MBC of P-U (C) and of P-Z (D) at 20% MOFs-Ag by weight of PVC.

The MICs and MBCs in this study are higher than the ones previously reported by our group for the freely suspended UiO-66(COOH)₂-Ag (MIC and MBC of 6.5 $\mu\text{g}/\text{mL}$ of silver content). Nevertheless, this observation further supports the contact-based mechanisms which are more pronounced in a suspension solution. It also validates the use of MOFs-Ag in membranes for their potential application in surgical masks and antibacterial films, which would not have been possible if the main mechanisms of antibacterial activities are based on the release of Ag cations.

To further validate the efficacy of the membranes, the antibacterial activity of PVC fibers prepared with silver nitrate P-A is assessed. At 5% AgNO₃ by weight of PVC, we observed 54% bacterial inhibition with effective inhibition of 0.84. At 10%, P-A showed a bacterial inhibition of 91% with effective inhibition of 0.40, and when

increased to 20% the MOFs-based membranes showed a 95% inhibition and an EI of 0.24 (Figure 17).

Moreover, P-A at 20% showed an MIC of 26 $\mu\text{g/mL}$ and an MBC of 66 $\mu\text{g/mL}$ (Figure 17). While the calculated MIC was better than those of P-Z and P-U, the amount of silver used in P-A was substantially much higher. Indeed, the bactericidal effect was more comparable with the reported EIs where everything is equal and the silver concentration is normalized, P-Z and P-U demonstrated much higher effective inhibition.

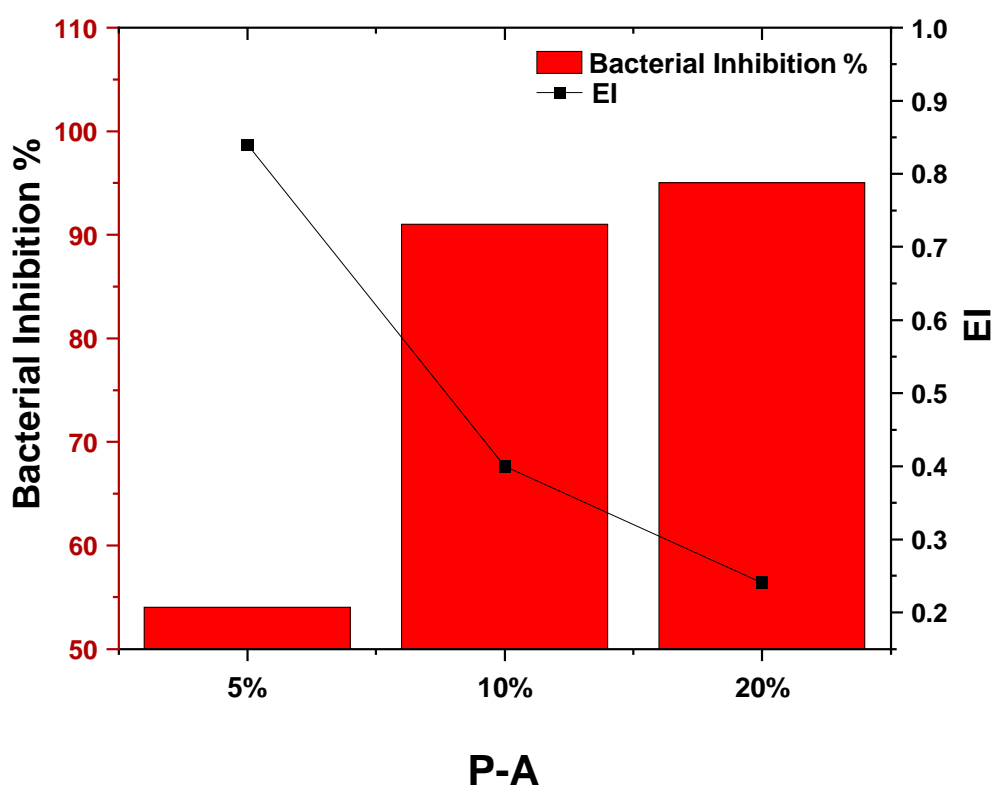


Figure 17 The Relationship between bacterial inhibition and EI for P-A

CHAPTER V

CONCLUSIONS AND PERSPECTIVES

In this study, electrospinning technique was used to produce three different membranes that are all made up of PVC polymer as the main matrix but the fillers are different which are ZIF-8-Ag, UiO-66(COOH)₂-Ag and AgNO₃. Briefly, the solutions were prepared by dissolving PVC powder in a mixture of DMF: THF then adding different percentages of the MOFs or AgNO₃ suspended solution to it. The solutions are then electrospun using parameters that ensure a stable jet on the top of the nozzle.

The produced membranes were then characterized, SEM images show that both MOFs were imbedded inside the fibers as clusters for UiO-66(COOH)₂-Ag, and solely for ZIF-8, while for AgNO₃ no major change in the morphology was observed. The fiber diameter did not effectively change for the case of PVC/UiO-66(COOH)₂-Ag and PVC/AgNO₃ at 5 and 10% loading due to small MOFs size, but for PVC/ZIF-8-Ag the change in fiber diameter was noticeable. Almost all the membranes fiber diameter have changed at 20% loading and this can be related to the size of the MOFs and the change in the behavior of the solution at this high loading %. Capillary Flow Porometer was used to measure the pore size distributions and Liquid Entry Pressure (LEP) of the samples, PVC/AgNO₃ membranes did not show a noticeable change in pore size while for all other membranes with all different loadings the pore sizes have mostly increased but with different ways, LEP did not change for PVC/ZIF-8-Ag membranes in comparison with normal PVC membranes, but the presence of AgNO₃ and UiO66(COOH)₂-Ag had a big effect on the LEP of the corresponding membranes, this can be related to the roughness and pore size. Upon adding the MOFs and AgNO₃, we did not notice any effective change in the water contact angle (WCA) which is a good sign that the hydrophobicity is compromised. ThermoGravimetric analysis (TGA) demonstrated that PVC/ZIF-8-Ag had

the best thermal stability at high temperature among the other treated membranes in comparison with normal PVC, although UiO-66(COOH)₂-Ag MOF was more stable alone..

The anti-bacterial properties of the membranes have increased with the increase in silver loading in all the tested samples at mass of 15mg. In fact, it reached up to 95% bacterial inhibition in all samples for 20 % loading, but what is worth mentioning is that the MOFs-Ag based treatments have reached this inhibition in a much lower Ag loading percentage than that of AgNO₃ samples (0.93% for PVC/ZIF-8-Ag, 1.46% for PVC/UiO-66(COOH)₂-Ag & 7.94% for PVC/AgNO₃), this clearly demonstrates the importance of MOFs in this study as an anti-bacterial agent. The obtained results support a direct contact inhibition mechanism demonstrating the significance of the MOFs scaffolds in our designed membrane system. This work paves the way for the development of new applications for composite membranes prepared via electrospinning such as air filters.

In future work, the aim is to test the membranes as potential antibacterial air filters that are capable of filtering the air from particulate matter in addition to germs and bacteria even fungus to mimic high efficiency air filters such as HEPA Filters. In addition, it is important to test another types of polymers especially eco-friendly and biodegradable polymers. Moreover, testing different MOFs would be highly valuable for comparison and benchmarking.

REFERENCES

1. Fenger, J., *Air pollution in the last 50 years – From local to global*. Atmospheric Environment, 2009. **43**(1): p. 13-22.
2. Salthammer, T., *Emissions of Volatile Organic Compounds from Products and Materials in Indoor Environments*, in *Air Pollution: Indoor Air Pollution*, P. Pluschke, Editor. 2004, Springer Berlin Heidelberg: Berlin, Heidelberg. p. 37-71.
3. Fauci, A.S., N.A. Touchette, and G.K. Folkers, *Emerging infectious diseases: a 10-year perspective from the National Institute of Allergy and Infectious Diseases*. Emerg Infect Dis, 2005. **11**(4): p. 519-25.
4. Nicola, M., et al., *The socio-economic implications of the coronavirus pandemic (COVID-19): A review*. Int J Surg, 2020. **78**: p. 185-193.
5. Seidi, F., et al., *Functionalized Masks: Powerful Materials against COVID-19 and Future Pandemics*. Small, 2021. **17**(42): p. 2102453.
6. Narayan, Y., et al., *Assessing effectiveness and comfortability of a two-layer cloth mask with a high-efficiency particulate air (HEPA) insert to mitigate COVID-19 transmission*. Physics of Fluids, 2022. **34**(6): p. 061703.
7. Landry, S.A., et al., *Fit-tested N95 masks combined with portable HEPA filtration can protect against high aerosolized viral loads over prolonged periods at close range*. The Journal of Infectious Diseases, 2022: p. jiac195-jiac195.
8. Handbook, A., *HVAC systems and equipment*. Vol. 39. 1996: chapter.
9. Wang, S. and Z. Ma, *Supervisory and Optimal Control of Building HVAC Systems: A Review*. HVAC&R Research, 2008. **14**(1): p. 3-32.
10. Liu, G., et al., *A review of air filtration technologies for sustainable and healthy building ventilation*. Sustainable Cities and Society, 2017. **32**: p. 375-396.
11. Aquino, S., et al., *Analysis of fungal contamination in vehicle air filters and their impact as a bioaccumulator on indoor air quality*. Air Quality, Atmosphere & Health, 2018. **11**(10): p. 1143-1153.
12. Lee, L.D., et al., *Risk of Bioaerosol Contamination With Aspergillus Species Before and After Cleaning in Rooms Filtered With High-Efficiency Particulate Air Filters That House Patients With Hematologic Malignancy*. Infection Control & Hospital Epidemiology, 2007. **28**(9): p. 1066-1070.
13. Cho, K., et al. *Changes in Fan Energy Consumption According to Filters Installed in Residential Heat Recovery Ventilators in Korea*. Sustainability, 2021. **13**, DOI: 10.3390/su131810119.
14. Watson, R., et al., *Efficacy of antimicrobial and anti-viral coated air filters to prevent the spread of airborne pathogens*. Scientific Reports, 2022. **12**(1): p. 2803.
15. Akdere, M. and T. Schneiders, *9 - Modeling of the electrospinning process*, in *Advances in Modeling and Simulation in Textile Engineering*, N.T. Akankwasa and D. Veit, Editors. 2021, Woodhead Publishing. p. 237-253.
16. Im, J.S., et al., *The study of controlling pore size on electrospun carbon nanofibers for hydrogen adsorption*. Journal of Colloid and Interface Science, 2008. **318**(1): p. 42-49.
17. Li, H., et al. *Application of Electrospinning in Antibacterial Field*. Nanomaterials, 2021. **11**, DOI: 10.3390/nano11071822.

18. Alven, S., et al. *Electrospun Nanofibers/Nanofibrous Scaffolds Loaded with Silver Nanoparticles as Effective Antibacterial Wound Dressing Materials*. *Pharmaceutics*, 2021. **13**, DOI: 10.3390/pharmaceutics13070964.
19. Korber, B., et al., *Tracking Changes in SARS-CoV-2 Spike: Evidence that D614G Increases Infectivity of the COVID-19 Virus*. *Cell*, 2020. **182**(4): p. 812-827.e19.
20. Pullangott, G., et al., *A comprehensive review on antimicrobial face masks: an emerging weapon in fighting pandemics*. *RSC Advances*, 2021. **11**(12): p. 6544-6576.
21. Leung, N.H.L., et al., *Respiratory virus shedding in exhaled breath and efficacy of face masks*. *Nat Med*, 2020. **26**(5): p. 676-680.
22. Dr. Berlin, P.K., et al., *The Need of Understanding the Importance And Use Of Face Masks*. *Journal of Current Medical Research and Opinion*, 2021. **4**(02).
23. Feng, S., et al., *Rational use of face masks in the COVID-19 pandemic*. *The Lancet Respiratory Medicine*, 2020. **8**(5): p. 434-436.
24. Zhiqing, L., et al., *Surgical masks as source of bacterial contamination during operative procedures*. *J Orthop Translat*, 2018. **14**: p. 57-62.
25. Pasanen, A.L., et al., *Microbial growth on respirator filters from improper storage*. *Scand J Work Environ Health*, 1993. **19**(6): p. 421-5.
26. Zheng, C.R., et al., *Particulate Respirators Functionalized with Silver Nanoparticles Showed Excellent Real-Time Antimicrobial Effects against Pathogens*. *Environmental Science & Technology*, 2016. **50**(13): p. 7144-7151.
27. Fadare, O.O. and E.D. Okoffo, *Covid-19 face masks: A potential source of microplastic fibers in the environment*. *The Science of the total environment*, 2020. **737**: p. 140279-140279.
28. Rengasamy, S., E. Fisher, and R.E. Shaffer, *Evaluation of the survivability of MS2 viral aerosols deposited on filtering face piece respirator samples incorporating antimicrobial technologies*. *Am J Infect Control*, 2010. **38**(1): p. 9-17.
29. James, S.L., *Metal-organic frameworks*. *Chemical Society Reviews*, 2003. **32**(5): p. 276-288.
30. Li, R., T. Chen, and X. Pan, *Metal–Organic-Framework-Based Materials for Antimicrobial Applications*. *ACS Nano*, 2021. **15**(3): p. 3808-3848.
31. Mortada, B., et al., *Postmetalated Zirconium Metal Organic Frameworks as a Highly Potent Bactericide*. *Inorganic Chemistry*, 2017. **56**(8): p. 4739-4744.
32. Givirovskaia, D., et al., *Modification of face masks with zeolite imidazolate framework-8: A tool for hindering the spread of COVID-19 infection*. *Microporous and Mesoporous Materials*, 2022. **334**: p. 111760.
33. Azócar, M.I., et al., *Review: Antibacterial behavior of carboxylate silver(I) complexes*. *Journal of Coordination Chemistry*, 2014. **67**(23-24): p. 3840-3853.
34. Yin, I.X., et al., *The Antibacterial Mechanism of Silver Nanoparticles and Its Application in Dentistry*. *Int J Nanomedicine*, 2020. **15**: p. 2555-2562.
35. Khorrami, S., et al., *Selective cytotoxicity of green synthesized silver nanoparticles against the MCF-7 tumor cell line and their enhanced antioxidant and antimicrobial properties*. *Int J Nanomedicine*, 2018. **13**: p. 8013-8024.
36. Yiğit, B., et al., *Synthesis and antimicrobial studies of 1-methyl-2-dimethylaminoethyl-substituted benzimidazolium salts and N-heterocyclic carbene–silver complexes*. *Journal of Coordination Chemistry*, 2012. **65**(3): p. 371-379.

37. Heo, D.Y., et al., *Metal-Organic Framework Materials for Perovskite Solar Cells*. *Polymers*, 2020. **12**(9): p. 2061.
38. Naragund, V.S. and P.K. Panda, *Electrospun nanofiber-based respiratory face masks—a review*. *Emergent Materials*, 2022. **5**(2): p. 261-278.
39. Zhang, Z., et al., *Electrospun ultrafine fibers for advanced face masks*. *Mater Sci Eng R Rep*, 2021. **143**: p. 100594.
40. Zhang, R., et al., *Nanofiber Air Filters with High-Temperature Stability for Efficient PM_{2.5} Removal from the Pollution Sources*. *Nano Letters*, 2016. **16**(6): p. 3642-3649.
41. Gu, G.Q., et al., *Triboelectric Nanogenerator Enhanced Nanofiber Air Filters for Efficient Particulate Matter Removal*. *ACS Nano*, 2017. **11**(6): p. 6211-6217.
42. Zuo, F., et al., *Free-Standing Polyurethane Nanofiber/Nets Air Filters for Effective PM Capture*. *Small*, 2017. **13**(46): p. 1702139.
43. Simmons, R.B., et al., *Fungal Colonization of Air Filters from Hospitals*. *American Industrial Hygiene Association Journal*, 1997. **58**(12): p. 900-904.
44. Sublett, J.L., *Effectiveness of air filters and air cleaners in allergic respiratory diseases: a review of the recent literature*. *Current allergy and asthma reports*, 2011. **11**(5): p. 395-402.
45. American Society of Heating, R., and Air Conditioning Engineers (ASHRAE), *MERV, Air Filtration*. December 8, 2020.
46. (EPA), U.S.E.P.A. *What is a HEPA filter?* n.a; Available from: [https://www.epa.gov/indoor-air-quality-iaq/what-hepa-filter#:~:text=It%20is%20an%20acronym%20for,of%200.3%20microns%20\(%20B5m\)](https://www.epa.gov/indoor-air-quality-iaq/what-hepa-filter#:~:text=It%20is%20an%20acronym%20for,of%200.3%20microns%20(%20B5m).).
47. Saliba, D., et al., *Crystal Growth of ZIF-8, ZIF-67, and Their Mixed-Metal Derivatives*. *Journal of the American Chemical Society*, 2018. **140**(5): p. 1812-1823.
48. Bin, Q., M. Wang, and L. Wang, *Ag nanoparticles decorated into metal-organic framework (Ag NPs/ZIF-8) for electrochemical sensing of chloride ion*. *Nanotechnology*, 2020. **31**(12): p. 125601.
49. Beachley, V. and X. Wen, *Effect of electrospinning parameters on the nanofiber diameter and length*. *Mater Sci Eng C Mater Biol Appl*, 2009. **29**(3): p. 663-668.
50. Najafi, S.J., et al., *The effect of electrospinning parameters on the morphology of glass nanofibers*. *The Journal of The Textile Institute*, 2020. **111**(7): p. 941-949.
51. Morais, S., *Porosity of fiber mats from different polymer solutions - evaluating the influence of process and solution parameters*. 2011.
52. Alghoraibi, I., *Different methods for nanofibers design and fabrication*. 2018.
53. Wiegand, I., K. Hilpert, and R.E.W. Hancock, *Agar and broth dilution methods to determine the minimal inhibitory concentration (MIC) of antimicrobial substances*. *Nature Protocols*, 2008. **3**(2): p. 163-175.
54. Nelson, T., et al., *Electrospun composite polycaprolactone scaffolds for optimized tissue regeneration*. *Proceedings of the Institution of Mechanical Engineers, Part N: Journal of Nanoengineering and Nanosystems*, 2012. **226**: p. 111-121.
55. Alkhudhiri, A. and N. Hilal, *3 - Membrane distillation—Principles, applications, configurations, design, and implementation*, in *Emerging Technologies for Sustainable Desalination Handbook*, V.G. Gude, Editor. 2018, Butterworth-Heinemann. p. 55-106.

56. Qin, X.-H., et al., *Effect of different salts on electrospinning of polyacrylonitrile (PAN) polymer solution*. Journal of Applied Polymer Science, 2007. **103**(6): p. 3865-3870.
57. Topuz, F., et al., *Influence of salt addition on polymer-free electrospinning of cyclodextrin nanofibers*. Nano Express, 2020. **1**(2): p. 020041.
58. Topuz, F., et al., *Nanofiber engineering of microporous polyimides through electrospinning: Influence of electrospinning parameters and salt addition*. Materials & Design, 2021. **198**: p. 109280.
59. Fux, C.A., et al., *Survival strategies of infectious biofilms*. Trends in microbiology, 2005. **13**(1): p. 34-40.
60. Regiel, A., et al., *Preparation and characterization of chitosan–silver nanocomposite films and their antibacterial activity against Staphylococcus aureus*. Nanotechnology, 2012. **24**(1): p. 015101.
61. Bondarenko, O., et al., *Particle-cell contact enhances antibacterial activity of silver nanoparticles*. PloS one, 2013. **8**(5): p. e64060.